High-resolution mapping of the mobility–lifetime product in CdZnTe using a nuclear microprobe

2004 J. Phys.: Condens. Matter 16 S67

(http://iopscience.iop.org/0953-8984/16/2/008)

INSTITUTE OF PHYSICS PUBLISHING JOURNAL OF PHYSICS: CONDENSED MATTER

J. Phys.: Condens. Matter **16** (2004) S67–S73 PII: S0953-8984(04)66803-2

High-resolution mapping of the mobility–lifetime product in CdZnTe using a nuclear microprobe

A Lohstroh[1], **P J Sellin**[1] **and A Simon**[2,3]

[1] Department of Physics, University of Surrey, Guildford GU2 7XH, UK
[2] Surrey Centre for Ion Beam Applications, University of Surrey, Guildford GU2 7XH, UK

E-mail: P.Sellin@surrey.ac.uk

Received 31 July 2003
Published 22 December 2003
Online at stacks.iop.org/JPhysCM/16/S67 (DOI: 10.1088/0953-8984/16/2/008)

Abstract

We present frontal ion beam induced charge imaging on a cadmium zinc telluride device using a 2.05 MeV He microbeam. Two sets of voltage-dependent 3 mm × 3 mm scans over the device cathode were acquired at room temperature and 250 K respectively and the corresponding charge collection efficiency (CCE) images extracted. The reduction of CCE due to electron transport with reduced bias voltage can be described using a simplified Hecht equation. This allows us to measure the mobility–lifetime product for electrons ($\mu_e\tau_e$) and so produce high-resolution $\mu_e\tau_e$ images at 296 and 250 K. At 296 K, CCE values up to 96% were observed for an electric field of 3570 V cm^{-1}. In general, the CCE values at 250 K are lower than the comparable values at 296 K with $\mu_e\tau_e$ decreasing from 4.7×10^{-4} to 1.2×10^{-4} cm^2 V^{-1}, about 1/4 of its original value. Additionally, we observe an increase in CCE at 250 K due to previous irradiation of the material, caused by partial filling of electron traps by the ion beam.

1. Introduction

Cadmium zinc telluride (CZT) is a promising material for radiation detection applications. The advantages of high resistivity and low leakage current even at room temperature, and a high absorption cross section for x- and γ-rays make CZT a suitable candidate for portable detection systems and imaging arrays with spectroscopic properties [1]. To improve the spectroscopic performance, a detailed understanding of the parameters affecting the charge transport in the material is required and a lot of research is currently being carried out on CZT.

Ion beam induced charge (IBIC) imaging using a nuclear microprobe has been shown to be a powerful tool for the characterization of uniformity of detector response with micrometre

[3] On the leave from: Institute of Nuclear Research, Hungarian Academy of Sciences (ATOMKI), Debrecen, Hungary.

spatial resolution [2–5]. In this study we use the frontal IBIC technique to acquire voltage-dependent charge collection efficiency (CCE) images by scanning the device cathode at two different temperatures. Application of the Hecht equation to CCE images allows us to generate maps of the mobility–lifetime product ($\mu_e\tau_e$) [4, 6], which is an important parameter for the detection properties of the material. Specifically, we wanted to investigate the use of a nuclear microbeam to produce quantitative maps of $\mu_e\tau_e$ and so investigate any non-uniformity in the CZT material.

2. Experimental details and data analysis

The IBIC experiments described in this paper were performed at the University of Surrey microbeam, with 2.05 MeV He ions focused to a beam spot size of less than 4 μm diameter. The detector-grade single-crystalline $Cd_1Zn_{0.8}Te_{0.2}$ sample had a thickness of $d = 700$ μm. Ohmic gold contacts were evaporated onto the sample, forming a square 5 mm $\times$ 5 mm contact on the top surface and a planar contact on the back. The device was negatively biased and irradiated through the top contact. The ion beam raster scans over the cathode at a rate of 500 μs/pixel. The induced charge signal was amplified by a charge-sensitive preamplifier and a shaping amplifier (shaping time = 0.5 μs). The resulting pulses were digitized by a multichannel analyser (MCA) and stored as event by event data [7]. The electronic noise measured from our sample was below the MCA threshold. This threshold implies that we were insensitive to events below 8% CCE.

We acquired voltage-dependent IBIC images in 50 V steps from -50 up to -250 V bias voltage at sample temperatures of 296 and 250 K, each with a scanning area of 3 mm $\times$ 3 mm. At 250 K a 270 μm $\times$ 270 μm scan was also carried out to reveal more spatial detail. The sample was mounted on a temperature-controlled copper cold finger, cooled with liquid nitrogen.

The induced charge signal measured from the CZT sample was calibrated using a Si detector with a nominal CCE of 100% using electron–hole pair creation energies of 3.6 and 4.4 eV for silicon [8] and CZT [3, 9] respectively. The event rate on the sample was typically 1500–2000 Hz and each image of 256 $\times$ 256 pixels was acquired for 12 min, yielding $\approx$40 events/pixel. CCE maps were produced by calculating the mean value of the pulse height spectra at each pixel position.

The interaction depth of the He ion, $x = 4.7$ μm, is determined using TRIM [10]. The charges are created close to the cathode and the induced charge signal originates from electrons moving to the anode. The variation of CCE with bias voltage can be described by the simplified Hecht equation (1) under the assumption of a homogeneous electric field $E = V/d$ and a negligible contribution of holes to the induced charge signal [8, 11]

$$\mathrm{CCE} = \frac{\mu_e\tau_e E}{d}\left[1 - \exp\left(-\left(1 - \frac{x}{d}\right)\left(\frac{\mu_e\tau_e E}{d}\right)^{-1}\right)\right]. \quad (1)$$

CCE images were acquired at five different bias voltages. We obtained a set of voltage versus CCE data for each pixel position and extracted $\mu_e\tau_e$ by fitting these data sets to equation (1) using a Levenberg–Marquardt algorithm, yielding $\mu_e\tau_e$ images.

3. Results and discussion

Figure 1 shows the CCE images of our sample biased at -250 V, whose main features are representative of all the maps acquired at these temperatures. The contour of the gold contact is clearly visible in all the images, as well as a long vertical scratch across the contact which can be seen by eye on the sample. Additionally, the images show a regular pattern of low-CCE

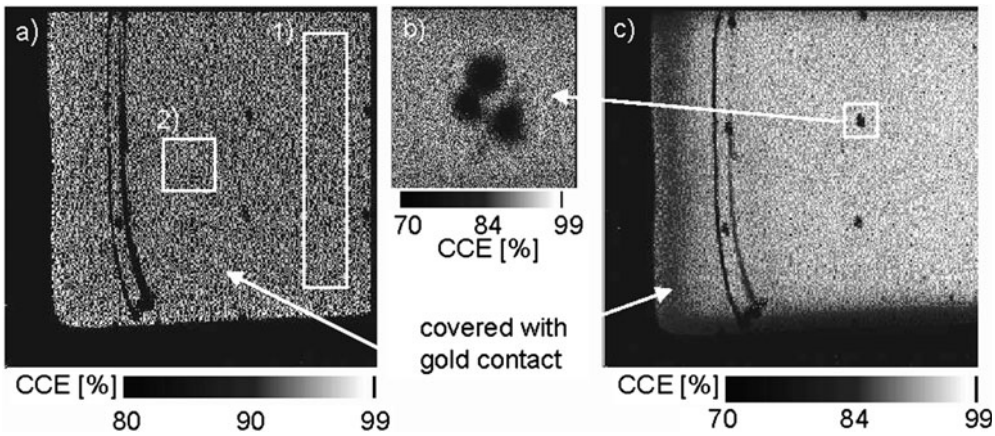

Figure 1. CCE images at a bias voltage of −250 V: (a) 3 mm × 3 mm scan at 296 K (the indicated areas are used for further analysis); (b) 270 μm × 270 μm scan of the indicated area in (c) at 250 K; (c) 3 mm × 3 mm scan at 250 K.

spots ≈1 mm apart from each other. These originate from a probing procedure which damaged the sample mechanically at these positions before deposition of the gold contact. The higher resolution 270 μm × 270 μm scan shows the three-dot structure of these probe marks more clearly. Apart from these damaged regions, the spatial distribution of CCE across the device at 296 K is very homogeneous. At 250 K the maximum CCE is found in a rectangular-shaped region at the right-hand side. Additionally, diagonal lines of slightly reduced CCE which are present at 296 K are not resolved at 250 K. The CCE generally decreases over the whole area with reducing bias, as expected from the Hecht equation. Reducing the temperature also leads to a reduction of CCE over the whole area, but instead of the evenly distributed values at 296 K, the images show an increasing trend from the left-hand side to the right-hand side.

The pulse height spectra obtained from the whole scanning area are shown in figure 2. They show various features corresponding to different regions of the sample. The full width at half-maximum (FWHM) of the main peak is constant at both temperatures at bias voltages from −250 to −150 V and increases at lower bias values. The resolution FWHM degrades from $1.2 \pm 0.2\%$ at high biases to $4.6 \pm 0.4\%$ at −50 V at 296 K and from $3.6 \pm 0.4\%$ to $6.1 \pm 0.6\%$ at 250 K. A separate set of data was acquired with the polarity of the sample bias reversed, so that the ion beam irradiated the anode. In this configuration, where the observed signal is due to hole transport in the CZT, hardly any pulses were observed above our MCA threshold. This behaviour is expected since the charge collection length λ_h of holes is short compared with the thickness of our detector, due to the short $\mu_h\tau_h$ [1].

The sequence of five CCE images acquired at the different voltages was used to produce the $\mu_e\tau_e$ images shown in figure 3. Each pixel in figure 3 represents the $\mu_e\tau_e$ value obtained from a fit to equation (1). Pixels with high χ^2 values, corresponding to data which do not provide a good fit to equation (1), are shown in white. They appear mainly in regions with low statistics due to only a few registered events. The distribution of $\mu_e\tau_e$ follows the same pattern which is expected from the CCE maps. Typically, values of $\mu_e\tau_e$ at 250 K are reduced to ≈25% of their value at 296 K, e.g. $\mu_e\tau_e = 4.7 \times 10^{-4}$ and 1.2×10^{-4} cm^2 V^{-1} respectively (figure 4).

The $\mu_e\tau_e$ images at the two different temperatures differ significantly in quality, which reflects the accuracy of the fitted data. At 296 K the reduction of CCE between −250 and −50 V is only about 5% and the fit is very sensitive to statistical fluctuations of the CCE values

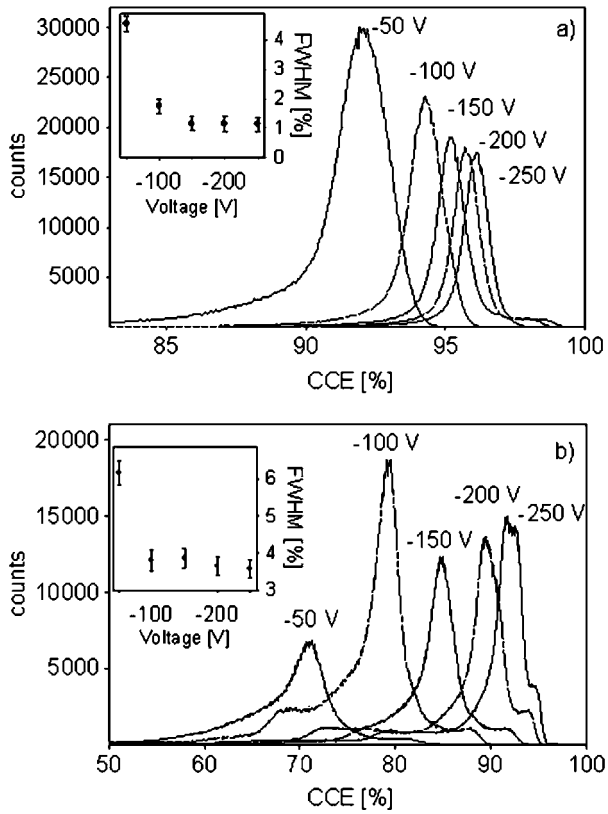

Figure 2. Pulse height spectra of the 3 mm × 3 mm scan area at the indicated bias voltages, the inset shows the FWHM/peak centroid ratio: (a) at 296 K, (b) at 250 K.

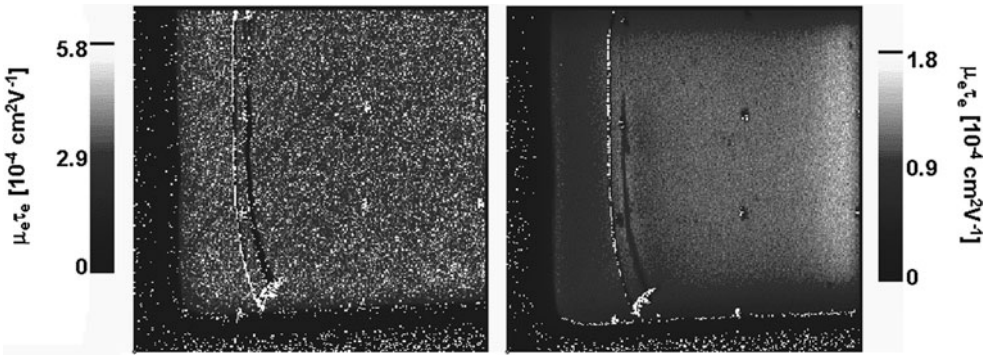

Figure 3. $\mu_e\tau_e$ images of the 3 mm × 3 mm scan area: left, 296 K; right, 250 K.

in each pixel, which can be of the same magnitude as the observed change in CCE with bias voltage. This leads to a broad distribution of $\mu_e\tau_e$ values within a few pixels, which has no physical significance. In contrast, at 250 K larger changes in CCE are observed and the resulting fit to equation (1) is less affected by statistical fluctuations. However, it is evident that the CCE is evenly distributed at 296 K. The 250 K images show a distinct region of high $\mu_e\tau_e$ at the right-hand side.

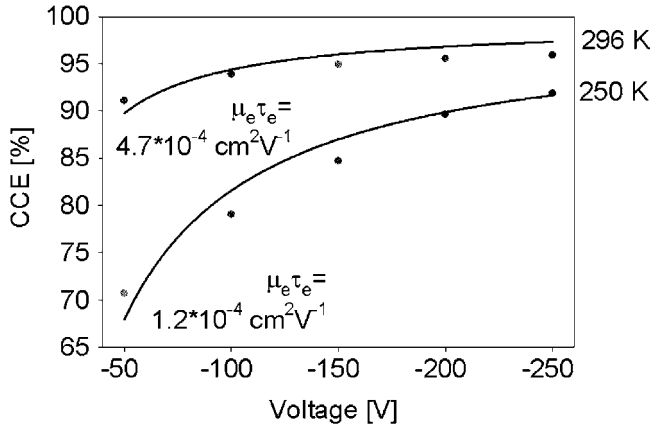

Figure 4. Peak centroids of the pulse height spectra in figure 2 versus bias voltage. The curves show fits to the Hecht equation (1).

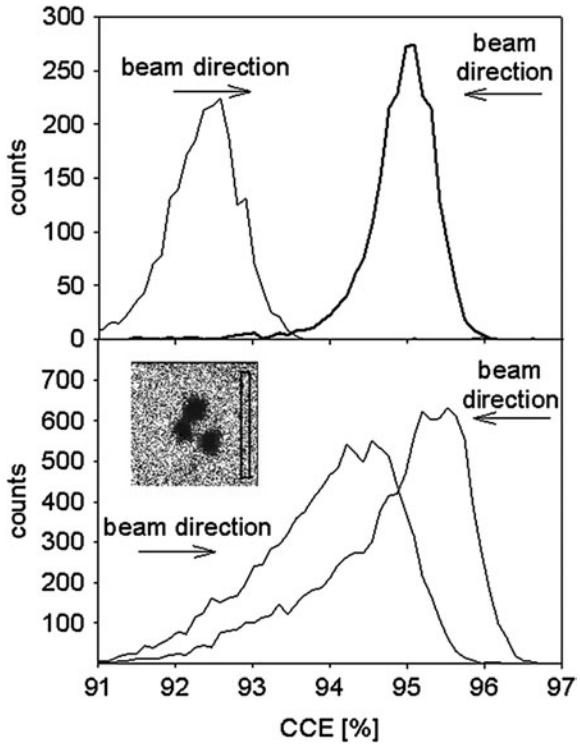

Figure 5. Pulse height spectra of a single movement of the beam over the sample area, resolved in the two different directions of scanning movement of the ion beam: top, extracted from area (1) indicated in figure 1; bottom, extracted from the indicated area as shown in the inset of the 270 μm $\times$ 270 μm data.

Schlesinger *et al* [1] report that the resolution of a CZT detector in α-particle spectroscopy is not affected by variations in electron drift length λ_e within 10%, if λ_e is large compared with the detector thickness. This corresponds to our constant resolution observed at 296 K between -250 and -150 V, which corresponds to λ_e between 1.7 and 1 mm.

The pulse height spectrum (figure 5, top) for the selected area marked as (1) in figure 1(a), clearly shows two separate peaks at 250 K independent of bias voltage. The separation of the two peak centroids increases with decreasing bias voltage from 3% CCE at −250 V to 9%. The effect is not found at 296 K. Further analysis reveals that the lower peak occurs when the scanning beam hits the region for the first time during the scan. The higher peak occurs after the ion beam reached the edge of the image and scans back over the same area. The effect occurs consistently throughout the 250 K data sets. In contrast the pulse height spectrum projected from region 2 contains only counts corresponding to the lower CCE peak. The data from the smaller scan show a similar effect, but the separation of the two peaks is reduced (figure 5, bottom). These data show that the CZT signal amplitude increases when scanned with the beam shortly after a previous event. This indicates priming of the material by the ion beam, due to filling of electron traps. The traps release the electrons with a time constant of the order of several tens of seconds, which will lead to a lower electron lifetime (and thus lower CCE), as observed in our data. Fitting the two peak positions yields an increase of $\mu_e\tau_e$ from 1.1×10^{-4} to 2.0×10^{-4} cm^2 V^{-1}. Medunić *et al* [3] also suggest an electron trapping–detrapping mechanism to be responsible for an increasing signal amplitude with measuring time. Due to the dependence of CCE on previous irradiation, the trapping–detrapping mechanism partly determines the resolution of the device. Toney *et al* [12] calculated the variation of resolution with temperature taking into account the changes in band gap and leakage current. Their result yields 250 K as a better operating temperature for CZT than 296 K if trapping is not taking into account. Our result shows that the resolution is potentially rate dependent at 250 K due to trap priming effects.

4. Conclusions

We applied the frontal IBIC imaging technique to investigate a 700 μm thick planar CZT device using cathode irradiation with 2.05 MeV He ions. CCE and $\mu_e\tau_e$ images show that mechanical damage strongly affects the detector performance at the damaged regions. The investigated material shows a uniform response at 296 K, close to 100% CCE at an electric field of 3570 V cm^{-1}. The CCE reduces at lower temperature and the resolution of the detector drops. The decrease in CCE with bias voltages can be described by the Hecht equation, which allows us to calculate quantitative $\mu_e\tau_e$ images by fitting the voltage dependent CCE data, extracted from each pixel position in the CCE maps. At 250 K the device shows 25% of its value at 296 K. Finally, we observed an electron trapping effect in the 250 K data. The signal amplitude increases if the area had been irradiated a few seconds previously. This will affect the energy resolution of the device, dependent on the applied dose rate.

Acknowledgments

This work was funded by EPSRC Instrument Development grant GR/R34486/01. AS was funded by EPSRC grant GR/RN0011.

References

[1] Schlesinger T E, Toney J E, Yoon H, Lee E Y, Brunett B A, Franks L and James R B 2001 *Mater. Sci. Eng.* **32** 103

[2] Rath S, Sellin P J, Breese M B H, Herman H, Alves L C and Holland A H 2003 Microscopic evaluation of spatial variations in material and charge transport properties of CdZnTe radiation detectors *Nucl. Instrum. Methods* A **512** 427

[3] Medunić Z, Jakšić M, Pastuović Ž and Skukan N 2003 *Nucl. Instrum. Methods* B **210** 237

[4] Vízkelethy G, Brunett B A, Walsh D S, James R B, Olsen R W and Doyle B L 1999 *Nucl. Instrum. Methods* B **158** 437
[5] Pastuović Ž and Jakšić M 2001 *Nucl. Instrum. Methods* B **181** 344
[6] Van Scyoc J M, Brunett B A, Yoon H, Gilbert T S, Hilton N R, Lund J C and James R B 1999 *Nucl. Instrum. Methods* A **428** 1
[7] Breese M B H, Jamieson N D and King P J C 1996 *Materials Analysis Using a Nuclear Microprobe* (New York: Wiley)
[8] Knoll G F 1999 *Radiation Detection and Measurement* 3rd edn (New York: Wiley)
[9] He Z and Knoll G F 1997 *Nucl. Instrum. Methods* A **388** 180
[10] Biersack J P and Haggmark L 1980 *Nucl. Instrum. Methods* **174** 257
[11] Hecht K 1932 *Z. Phys.* **77** 235
[12] Toney J E, Schlesinger T E and James R B 1999 *Nucl. Instrum. Methods* A **428** 14